A continuum model of colloid-stabilized interfaces

Sebastian Aland,[1] John Lowengrub,[2,3] and Axel Voigt[1,4]
[1]*Institut für Wissenschaftliches Rechnen, Technische Universität Dresden, 01062 Dresden, Germany*
[2]*Department of Mathematics, University of California, Irvine, Irvine, California 92697-3875, USA*
[3]*Department of Chemical Engineering and Materials Science, University of California, Irvine, Irvine, California 92697-3875, USA*
[4]*Center of Advanced Modeling and Simulation, Technische Universität Dresden, 01062 Dresden, Germany*

(Received 12 October 2010; accepted 12 April 2011; published online 17 June 2011)

Colloids that are partially wetted by two immiscible fluids can become confined to fluid-fluid interfaces. At sufficiently high volume fractions, the colloids may jam and the interface may crystallize. Examples include bicontinuous interfacially jammed emulsion gels (bijels), which were proposed in this study by Stratford *et al.* [Science **309**, 2198 (2005)] as a hypothetical new class of soft materials in which interpenetrating, continuous domains of two immiscible viscous fluids are maintained in a rigid state by a jammed layer of colloidal particles at their interface. We develop a continuum model for such a system that is capable of simulating the long-time evolution. A Navier-Stokes-Cahn-Hilliard model for the macroscopic two-phase flow system is combined with a surface phase-field-crystal model for the microscopic colloidal system along the interface. The presence of colloids introduces elastic forces at the interface between the two immiscible fluid phases. An adaptive finite element method is used to solve the model numerically. Using a variety of flow configurations in two dimensions, we demonstrate that as colloids jam on the interface and the interface crystallizes, the elastic force may be strong enough to make the interface sufficiently rigid to resist external forces, such as an applied shear flow, as well as surface tension induced coarsening in bicontinuous structures. © *2011 American Institute of Physics*.
[doi:10.1063/1.3584815]

I. INTRODUCTION

Like surfactants, colloidal particles that are partially wetted by two immiscible fluids tend to adsorb at the interface between the fluids to minimize the overall free energy of the system. However, there are important differences between the behavior of interfaces covered with surfactants and those covered with colloids. In the case of surfactants, if the interface area is changed, surfactants adsorb to and desorb from an interface and try to maintain an equilibrium surface tension. However, in the case of colloids, the desorption energy is typically much larger than the thermal energy, and thus the adsorption process of the colloids at the interface is practically irreversible. Therefore, a decrease in interfacial area leads to an energy increase because colloids have to desorb from the interface. On the other hand, an increase in interfacial area also leads to an overall increase in energy as the interface becomes more exposed by reducing the surface colloid fraction. Because the surface tension is the variation of the free energy with respect to interfacial area, this suggests that surface colloids are better described using an interfacial elasticity model rather than a surface tension model that is more suitable for surfactants (see, for example, Refs. 1 and 2).

As the colloid density at an interface increases, e.g., through the adsorption of colloids or through a reduction in interface area, the colloids may crowd and become immobilized forming a jammed colloidal monolayer. The crystallized interface can be solid-like with mechanical rigidity. This ability to impart rigidity and surface elasticity is an important difference between surface colloid and surfactant systems. In particular, unlike surfactants, colloid jamming can lead to interfaces with unusual shapes such as nonspherical bubbles[3] and unusual fluid configurations such as stabilized (Pickering) emulsions[2,4–7] and bicontinuous morphologies.[2,8] Stable bicontinuous morphologies in which interpenetrating, continuous domains of two immiscible fluids are maintained in a rigid state by a jammed layer of colloidal particles at their interface were discovered several years ago by Chung *et al.*[9] experimentally for thin films of polymeric fluids and by Stratford *et al.*[10] numerically for viscous fluids. Stratford *et al.* referred to such configurations as bicontinuous interfacially jammed emulsion gels (bijels) and proposed that bijels form a new class of soft materials with potentially remarkable properties with elastic moduli and yield stress tunable over a very wide range. Such structures have wide variety of potential applications including barrier materials,[11] solar cells,[12] food systems,[7] crossflow microreactors,[10] and as template scaffolds for colloidal gels.[13] Experiments recently performed by Herzig *et al.*[14] have demonstrated the ability to produce three dimensional bijels using viscous fluids that are stable for several months. Bijels have also been recently produced using biopolymers.[15]

As mentioned above, bijels were first discovered using numerical simulations by Stratford *et al.*[10] for equal volume fractions of the two fluid components. Later simulations were performed by Kim *et al.*[16] to determine the effect of varying volume fraction. These authors used a lattice Boltzmann method (LBM) with colloids undergoing Brownian motion. The wide range of spatiotemporal scales makes this

problem very difficult to solve. The spatial scales that need to be resolved range from the inter-colloid forces in the jammed layer on the interface to the mesoscopic bicontinuous domain structures that characterize the bijel. The time scales range from those associated with the Brownian motion of the colloids to the macroscopic arrest of the structure, which can last up to several months.[14] In the LBM, resolving this range of time scales is particularly problematic since the simulation time is limited by the Brownian diffusion time making it difficult to perform long-time simulations. Hore and Laradji,[17] using another approach based on dissipative particle dynamics (DPD), confirmed the results of Stratford *et al*. and predicted that bijels are thermodynamically metastable with smaller colloids being more easily desorbed which destabilizes the structure. In the DPD approach, colloids are modeled by arranging DPD particles on a sphere and connecting them by rigid bonds taking care that fluid particles cannot penetrate. This limits the size of the colloids and the range of spatial scales that can be simulated.

Here, we develop an alternative modeling approach, which combines the atomistic processes along the interface with the continuum processes in the bulk phases, that has the potential to simulate large domains for long times. In particular, we develop a continuum model that combines diffuse-interface (phase-field) modeling for multiphase flow with approximations to dynamic density functional theory (DDFT) to study colloid jamming at interfaces. DDFT is a time-dependent extension of classical (equilibrium) density functional theory and describes the time evolution of the density of interacting Brownian particles through an integro-differential equation (e.g., see Refs. 18 and 19). Classical density functional theory has been previously used for determining equilibria in one dimension of mixtures of amphiphilic particles (e.g., see Refs. 20 and 21) and for modeling colloidal fluids (e.g., see Refs. 18 and 22). In the DDFT, the dynamic integro-differential equations for the particle density can be derived from Newton's equations of motion with and without inertial effects. In recent work, van Teeffelen *et al*.[23] derived a local higher order partial differential equation for the colloid particle density by approximating the integro-differential equation of the DDFT model. The resulting partial differential equation is the so-called phase-field-crystal (PFC) model, which was previously introduced by Elder *et al*.[24,25] in the context of crystal growth. As the model resolves each particle as a density peak, it requires sub-particle resolution. However, the model operates on diffusive time scales, which enables the approach to resolve the long term behavior of the system. The PFC model has been used to describe various solid state phenomena (see, for example, Refs. 26 and 27). In very recent work, Backofen *et al*.[28] modified the PFC model to describe crystallography on fixed, curved surfaces which is related to the ordering of colloids on fluid-fluid interfaces. However, Backofen *et al*. did not consider interfacial motion or interactions with the bulk fluids. Here, we develop a surface phase-field-crystal (SPFC) model that accounts for these additional effects to model the jamming of colloidal particles on fluid-fluid interfaces. We also develop a model for attachment of colloids to the interface. A concentration equation for a colloidal density in one fluid phase is used with attachment/detachment boundary conditions along the fluid-fluid interface. These surface and bulk equations are reformulated using the diffuse interface and diffuse domain approaches introduced in Refs. 29–31 for solving partial differential equations on surfaces and complex domains and coupling surface and bulk problems. These techniques were recently used to simulate the effect of soluble surfactants on interfacial flows.[32]

To model the fluid flow, the incompressible Navier-Stokes equations used together with a diffuse interface (phase-field) approach. This method has a long history dating back to van der Waals and has been used for a wide variety of applications involving drop coalescence and break-up, spinodal decomposition, electrowetting, viscoelasticity, surfactants, etc. See, for example, the reviews[33–35] and the references therein. In this approach, an auxiliary phase-field (PF) function is introduced, which approximates the concentration of one of the fluid components. Interfaces are replaced by narrow diffuse layers across which the PF function varies from zero to one. Extra stresses in the fluid arise due to the presence of interfaces and colloids.

The governing equations, and extra stresses, are derived using an energy variation approach accounting for surface energy, modeled by a Cahn-Hilliard (CH)-type energy,[36] and the energy associated with surface colloids from the SPFC model. It is seen that the latter introduces elastic forces in the fluid. The resulting Navier-Stokes-Cahn-Hilliard-Surface-Phase-Field-Crystal (NSCHSPFC) equations are discretized using adaptive finite elements in space and a semi-implicit time-discretization. Using a variety of flow configurations in two dimensions, we demonstrate that as colloids jam on the interface and the interface crystallizes, the elastic force may be strong enough to make the interface sufficiently rigid to resist external forces, such as an applied shear flow, as well as surface tension induced coarsening in bicontinuous structures.

The paper is organized as follows. In Sec. II , we derive the model using an energy variation argument. In Sec. III, the numerical method is briefly described, and in Sec. IV, we show simulation results. Conclusions are drawn in Sec. V.

II. MODEL

A. Model derivation

In this section, we derive the governing equations using an energy variation approach. We do this in nondimensional variables where time and space are nondimensionalized by $t' = t/\tau_\sigma$ and $x' = x/L$ where $\tau_\sigma = \sqrt{\bar{\rho}L^3/\sigma}$ is the characteristic time associated with surface tension relaxation, with σ being the surface tension and $\bar{\rho}$ the density of the fluid, which is assumed to be constant. The parameter L is a measure of the characteristic size of the fluid domain (e.g., drop radius, etc.). We refer the reader to the Appendix for details. Hereafter, we drop the prime notation.

We begin by briefly reviewing the PFC model for bulk systems. Let ρ denote the nondimensional colloid density. Then the PFC model describes the conserved dynamics arising from a Swift-Hohenberg (SH)-like energy[37]

$\frac{\partial \rho}{\partial t} = \nabla \cdot \left(M \nabla \frac{\delta E_{SH}}{\delta \rho} \right)$ where M is a mobility, $\frac{\delta E_{SH}}{\delta \rho}$ denotes the variational derivative of the SH-like energy E_{SH} with respect to ρ. In nondimensional form, E_{SH} is given by

$$E_{SH} = El^{-1} \int f_{pfc}(\rho, \nabla\rho, \nabla^2\rho)\, dx, \quad f_{pfc}(\rho, \nabla\rho, \nabla^2\rho) = \frac{\rho^4}{4} + \frac{\rho^2}{2}(1+r) - \delta^2 |\nabla\rho|^2 + \frac{\delta^4}{2} |\nabla^2 \rho|^2, \tag{1}$$

where El is an elasticity number which measures the relative strength of the elastic energy (to the surface energy), f_{pfc} is the colloid energy density, r is a nondimensional parameter that arises from the structure factor for the colloidal system, and $\delta = L_c/L$ is the ratio of the characteristic length scales of the colloid and fluid systems. Again, we refer the reader to the Appendix for details. The energy E_{SH} is different from the standard Cahn-Hilliard types of energies (e.g., see Eq. (9) below) in that in addition to constant states, E_{SH} admits periodic solutions as equilibria, courtesy of the negative term involving the gradient of ρ. These periodic solutions describe the arrangement of colloids in the crystallized (ordered) state. For example, taking $r = -0.4$ the crystal state occurs when $\rho \approx 0$ The constant states describe the disordered or liquid states.

Next, we introduce E_{spfc} to be the localization of E_{SH} on a surface Γ using the diffuse interface formulation[29,31] as follows. To describe the position of the fluid-fluid interface Γ and of the two fluid phases, we use a phase field variable ψ such that $\psi = 0$ and 1 denote the fluid phases and $\psi = 0.5$ denotes the interface location $\Gamma(t) = \{\mathbf{x} \in \Omega : \psi(\mathbf{x}, t) = 0.5\}$ with $\Omega \subset I\ R^{2,3}$. For example, one may take

$$\psi(\mathbf{x}, t) = \frac{1}{2}\left[1 - \tanh\left(\frac{d(\mathbf{x}, t)}{\sqrt{2}\epsilon}\right)\right] \tag{2}$$

where ϵ determines the interface thickness and $d(\mathbf{x}, t)$ denotes the signed distance function from the fluid-fluid interface to $\mathbf{x}$ at time t. For this choice of ψ a calculation shows that the function

$$B(\psi) = \psi^2 (1-\psi)^2, \tag{3}$$

when scaled by $6\sqrt{2}/\epsilon$ approximates the surface delta function δ_Γ

$$\frac{6\sqrt{2}}{\epsilon} B(\psi) \approx \delta_\Gamma. \tag{4}$$

As discussed below, rather than using Eq. (2) to define ψ we determine ψ by solving an advective Cahn-Hilliard equation whose solution near Γ approximates Eq. (2) for small ϵ. The localized PFC energy on the surface, e.g., the SPFC energy, can then be written as

$$E_{spfc} = \frac{El^{-1}}{\epsilon} \int_\Omega B(\psi) f(\rho, \nabla\rho, v)\, dx, \tag{5}$$

where $f(\rho, \nabla\rho, v)$ is the SPFC energy density given by

$$f(\rho, \nabla\rho, v) = \frac{1}{4}\rho^4 + \frac{1+r}{2}\rho^2 - \delta^2 |\nabla\rho|^2 + \frac{\delta^4}{2} v^2, \tag{6}$$

$$v = \frac{1}{B} \nabla \cdot (B \nabla \rho). \tag{7}$$

We now suppose that the total energy of the system consists of the SPFC energy, the surface energy E_s and the kinetic energy E_{kin}

$$E = E_{spfc} + E_s + E_{kin}, \tag{8}$$

where in nondimensional form the surface energy is approximated by the Cahn-Hilliard energy

$$E_s = \frac{1}{\epsilon} \int_\Omega B(\psi) + \frac{\epsilon^2}{2} |\nabla\psi|^2\, dx, \tag{9}$$

where we do not enforce Eq. (2), and the kinetic energy is

$$E_{kin} = \frac{1}{2} \int_\Omega |\mathbf{u}|^2 dx, \tag{10}$$

where we have assumed that the density of the fluid is constant and the velocity is nondimensionalized by $U = L/\tau_\sigma$ (see the Appendix).

We now derive the equations for the two-phase system with colloidal particles starting with an energy variation argument. We take the time derivative of the energy E which is equivalent to varying ψ and ρ simultaneously. This gives

$$\dot{E} = \int_\Omega \mathbf{u}\, \dot{\mathbf{u}} + \dot{\psi} \frac{\delta E}{\delta \psi} + \dot{\rho} B \frac{\delta E}{\delta \rho}\ dx \tag{11}$$

where the overdot denotes the time derivative and

$$\frac{\delta E}{\delta \psi} := \frac{El^{-1}}{\epsilon} B' \left(f - \delta^4 \nabla v \cdot \nabla\rho - \delta^4 v^2\right) + \frac{1}{\epsilon}\left(B' - \epsilon^2 \Delta\psi\right) \tag{12}$$

$$\frac{\delta E}{\delta \rho} := \frac{El^{-1}}{\epsilon} \left(\rho^3 + (1+r)\rho + 2\delta^2 v + \frac{\delta^4}{B} \nabla \cdot (B \nabla v)\right). \tag{13}$$

We suppose the fluid motion is governed by the Navier-Stokes equations which, in the nondimensional variables introduced here, is given by

$$\dot{\mathbf{u}} = -\mathbf{u} \cdot \nabla \mathbf{u} - \nabla p + \frac{1}{Re} \Delta \mathbf{u} + \mathbf{F}, \nabla \cdot\ \mathbf{u} = 0, \tag{14}$$

where p is the pressure and $Re = \bar{\rho} L U/\eta$ with η the viscosity, is the Reynolds number, and the force $\mathbf{F}$ is as yet unspecified. Note that if Re is small, the Stokes equations could be used instead of the Navier-Stokes equations and the analysis below remains valid.

The functions ψ and ρ are assumed to satisfy the conservation equations

$$\dot{\psi} = -\mathbf{u} \cdot \nabla\psi - \nabla \cdot \mathbf{J}_\psi \tag{15}$$

$$\frac{\partial}{\partial t}(B\rho) = -\nabla \cdot (B\rho \mathbf{u}) - \nabla \cdot \mathbf{J}_\rho \tag{16}$$

where the fluxes $\mathbf{J}_\rho$ and $\mathbf{J}_\psi$ have also not yet been specified. Note that Eq. (16) is the diffuse interface form of the surface mass conservation equation.[29,31] Using the incompressibility of the fluid and Eq. (15), Eq. (16) can be rewritten as

$$\dot{\rho} = -\mathbf{u}\cdot\nabla\rho + \frac{B'}{B}\rho\nabla\cdot\mathbf{J}_\psi - \frac{1}{B}\nabla\cdot\mathbf{J}_\rho\,. \tag{17}$$

Next, we determine $\mathbf{F}$, $\mathbf{J}_\psi$ and $\mathbf{J}_\rho$ to ensure that the energy is nonincreasing in time ensuring thermodynamic consistency. Inserting Eqs. (14), (15), and (17) into Eq. (11) and integrating by parts, the time derivative of the energy becomes

$$\dot{E} = -\frac{1}{Re}\int_\Omega \nabla\mathbf{u} : \nabla\mathbf{u}\,dx + \int \mathbf{u}\cdot\left(\mathbf{F} - \frac{\delta E}{\delta\psi}\nabla\psi - B\frac{\delta E}{\delta\rho}\nabla\rho\right)dx + \int \mathbf{J}_\psi\cdot\nabla\left(\frac{\delta E}{\delta\psi} - B'\rho\frac{\delta E}{\delta\rho}\right)dx + \int \mathbf{J}_\rho\cdot\nabla\frac{\delta E}{\delta\rho}dx.$$

In the above, we have assumed natural (or periodic) boundary conditions and dropped all the boundary terms. By taking

$$\mathbf{F} = \frac{\delta E}{\delta\psi}\nabla\psi + B\frac{\delta E}{\delta\rho}\nabla\rho, \tag{18}$$

$$\mathbf{J}_\psi = -Pe_\psi^{-1}\epsilon B\nabla\left(\frac{\delta E}{\delta\psi} - B'\rho\frac{\delta E}{\delta\rho}\right), \tag{19}$$

$$\mathbf{J}_\rho = -Pe_\rho^{-1}B\nabla\frac{\delta E}{\delta\rho}, \tag{20}$$

where Pe_ψ and Pe_ρ are Peclet numbers, we obtain $\dot{E}\le 0$

If the flux $\mathbf{J}_\psi$ as defined in Eq. (19) is used in the conservation equation (15), the resulting ψ does not provide a good description of the interface layer because of the contributions of E_{spfc} to the variational derivatives. In particular, unlike the hyperbolic tangent function in Eq. (2), the interface thickness is non-uniform, which can introduce spurious Marangoni-like velocities. Since the primary purpose of ψ is to track the two-phase interface, we simplify $\mathbf{J}_\psi$ and omit the terms dependent on E_{spfc} which gives the standard Cahn-Hilliard flux

$$\mathbf{J}_\psi = -Pe_\psi^{-1}\nabla\frac{\delta E_s}{\delta\psi} = -Pe_\psi^{-1}B\nabla\left(B' - \epsilon^2\Delta\psi\right). \tag{21}$$

Although the resulting system is no longer variational and does not necessarily decrease the energy, this effect tends to be higher order since away from the interface $B(\psi)\approx 0$ and near the interface ψ locally equilibrates yielding $B'(\psi) - \epsilon^2\Delta\psi \approx 0$ Note that if $\mathbf{J}_\psi \approx 0$ then $\dot{E}\le 0$ with $\mathbf{F}$ and $\mathbf{J}_\rho$ given in Eqs. (18) and (20).

Using Eqs. (12) and (13), the force $\mathbf{F}$ in the Navier-Stokes equation can be written as

$$\mathbf{F} = \frac{El^{-1}}{\epsilon}B'\nabla\psi(f - \nabla v\cdot\nabla\rho - v^2) + B\frac{\delta E}{\delta\rho}\nabla\rho + \frac{\delta E_s}{\delta\psi}\nabla\psi \tag{22}$$

$$= \frac{El^{-1}}{\epsilon}\nabla\left(B\left(f - \delta^4\nabla v\cdot\nabla\rho - \delta^4 v^2\right)\right) + \overline{\mathbf{F}}, \tag{23}$$

where

$$\overline{\mathbf{F}} = -\frac{El^{-1}}{\epsilon}B\nabla(f - \delta^4\nabla v\cdot\nabla\rho - \delta^4 v^2) + B\frac{\delta E}{\delta\rho}\nabla\rho + \frac{\delta E_s}{\delta\psi}\nabla\psi. \tag{24}$$

We refer to the first two terms of $\overline{\mathbf{F}}$ as the elastic force and to the last term as the surface tension, or capillary, force. Note that if $\rho\approx$ constant so that the colloids are in the disordered or liquid state, then the elastic force is nearly zero. Further, Eq. (24) suggests that in equilibrium the interface experiences colloid-induced elastic stress just as it does capillary stress.

In the Navier-Stokes equations (14), we may use the force $\overline{\mathbf{F}}$ rather than $\mathbf{F}$ by introducing a new pressure $\bar{p}$ as

$$\bar{p} := p - \frac{El^{-1}}{\epsilon}B(f - \delta^4\nabla v\cdot\nabla\rho - \delta^4 v^2).$$

Numerically, we find that using $\overline{\mathbf{F}}$ yields a more accurate solution than using $\mathbf{F}$.

B. Attachment of colloids

We next consider the attachment of colloids to the interface with the idea of using attachment to drive the colloid density on the interface into the crystal part of the PFC phase diagram to induce colloid jamming and interface crystallization. Here, we do this by introducing a nondimensional colloid density in the bulk, c, which satisfies a convection-diffusion equation with a flux boundary condition at the interface that describes colloid attachment and detachment. We note that there are many other ways this could be done. For example, the bulk PFC equation (recall Sec. II A) could be used instead. However, since we are most interested in the case in which the colloids only crystallize at the interface, and not in the bulk fluid regions, the advection-diffusion equation is likely sufficient.

Here, we present the equations in nondimensional form and use the diffuse interface framework developed in Ref. 32. For simplicity, we assume that the colloids are soluble only in the fluid phase $\psi\equiv 1$. This leads to the convection-diffusion equation

$$\partial_t(\psi c) + \nabla\cdot(\psi\mathbf{u}c) = Pe_c^{-1}\nabla\cdot(\psi\nabla c) - hj|\nabla\psi|, \tag{25}$$

where Pe_c is a Peclet number, h is the penetration depth, and j is the net flux of colloids to the interface. Note that $|\nabla\psi|\approx\delta_\Gamma$ the surface delta function. The net flux j must also be accounted for in the evolution of the surface colloid density ρ through the addition of a source. Therefore, Eq. (17) is modified accordingly as

$$\dot{\rho} = -\mathbf{u}\cdot\nabla\rho + \frac{B'}{B}\rho\nabla\cdot\mathbf{J}_\psi - \frac{1}{B}\nabla\cdot\mathbf{J}_\rho + Bj. \tag{26}$$

There are numerous ways of defining the source term j. In general, it is not clear how to couple the macroscopic density c with the microscopic density ρ. The usual way of defining the net flux for macroscopic quantities is to use the constitutive assumption

$$j := Bi\big(c(\rho_\infty - \rho) - k^{-1}\rho\big), \tag{27}$$

where Bi is a Biot number that measures the adsorption rate relative to the surface tension time scale τ_σ and k^{-1} measures the relative rates of desorption and adsorption. The density ρ_∞ is a saturation constant that is in the crystal phase of the phase diagram of the PFC. The use of Eq. (27) may introduce difficulties, however, when ρ is in the crystal phase of the PFC. In this case, ρ oscillates locally with each oscillation representing a colloidal particle. Hence, attachment at valleys of ρ may drive the peaks of ρ above ρ_∞ which results in detachment. However, as discussed in the introduction, the attachment process for colloids is essentially irreversible so that detachment should be very limited.

To avoid this behavior one could use the simple form

$$j := Bi\, c \tag{28}$$

making the attachment and detachment independent of ρ by postulating that every existing colloid in the bulk will attach to the interface. In this case, colloid saturation is reached when c is depleted.

Another way to overcome the oscillations of ρ and connect the macroscopic and microscopic bulk and surface colloid densities in Eq. (27) is to use an average $\langle\rho\rangle$ instead of the microscopic ρ in Eq. (27) and take

$$j := Bi\big(c(\rho_\infty - \langle\rho\rangle) - k^{-1}\langle\rho\rangle\big), \tag{29}$$

where $\langle\rho\rangle$ could be either a local or global average of ρ over the interface.

We have implemented all of the above formulations for the flux term j and observed that all of these formulations behave similarly, at least qualitatively. For the simulations presented in Sec. IV A, we use Eq. (27) for j.

C. Shifting the free energy

Interface coarsening provides another route to driving the surface colloid density ρ into the crystal part of the PFC phase diagram, leading to colloid jamming and interface crystallization. For example, if the fluid structure coarsens in time and the interface length decreases then, in the absence of attachment, the absolute value of ρ increases. This can bring ρ into the crystal phase of the SPFC and thus induces crystallization of the interface. To account for this, we shift the SPFC energy in Eq. (6) by taking

$$f = \frac{1}{4}(\rho - \tilde\rho)^4 + \frac{1+r}{2}(\rho - \tilde\rho)^2 - \delta^2|\nabla\rho|^2 + \frac{\delta^4}{2}v^2, \tag{30}$$

where $\tilde\rho$ is a constant. The definitions of the variational derivatives $\delta E/\delta\psi$ and $\delta E/\delta\rho$ change accordingly. Equation (30) agrees with Eq. (1) when $\tilde\rho = 0$. On the other hand, taking the parameter $r = -0.4$ then the crystal phase occurs when $\rho \approx \tilde\rho$. In our numerical examples, we use by default $\tilde\rho = 0$ and only set $\tilde\rho \neq 0$ to simulate the jamming of particles in Sec. IV D.

D. Summary of governing equations

Putting everything together, we now summarize the nondimensional NSCHSPFC equations and the associated boundary conditions. We write the equations as a system of 2nd order partial differential equations. The advective Cahn-Hilliard equation governs the motion of the two-phase interface

$$\partial_t\psi + \mathbf{u}\cdot\nabla\psi = Pe_\psi^{-1}\nabla\cdot(B\nabla\mu), \tag{31}$$

$$\mu = B'(\psi) - \epsilon^2\Delta\psi. \tag{32}$$

The surface phase-field-crystal equation on the diffuse interface defined by ψ governs the evolution of the surface colloids

$$\partial_t(B\rho) + \nabla\cdot(B\mathbf{u}\rho) = Pe_\rho^{-1}\nabla\cdot(B\nabla\omega) + Bj, \tag{33}$$

$$B\omega = B(\rho - \tilde\rho)\Big((\rho - \tilde\rho)^2 + 1 + r\Big) + 2\delta^2 Bv + \delta^4\nabla\cdot(B\nabla v), \tag{34}$$

$$Bv = \nabla\cdot(B\nabla\rho), \tag{35}$$

$$j = Bi\big(c(\rho_\infty - \rho) - k^{-1}\rho\big). \tag{36}$$

The bulk colloid density evolves according to the convection-diffusion equation

$$\partial_t(\psi c) + \nabla\cdot(\psi\mathbf{u}c) = Pe_c^{-1}\nabla\cdot(\psi\nabla c) - hj|\nabla\psi|. \tag{37}$$

Finally, the Navier-Stokes equations, with surface tension and elastic forces, governs the motion of the fluids

$$\nabla\cdot\mathbf{u} = 0, \tag{38}$$

$$\partial_t\mathbf{u} + (\mathbf{u}\cdot\nabla)\mathbf{u} = -\nabla\bar p + \frac{1}{Re}\Delta\mathbf{u} + \frac{1}{\epsilon}\mu\nabla\psi + \frac{El^{-1}}{\epsilon}B\big(\omega\nabla\rho - \nabla(f - \delta^4\nabla v\cdot\nabla\rho - \delta^4 v^2)\big). \tag{39}$$

The NSCHSPFC system is equipped with the initial conditions

$$\mathbf{u}(t=0,\mathbf{x}) = \mathbf{u}_0(\mathbf{x}), \psi(t=0,\mathbf{x}) = \psi_0(\mathbf{x}), \rho(t=0,\mathbf{x}) = \rho_0(\mathbf{x}), c(t=0,\mathbf{x}) = c_0(\mathbf{x}), \quad \text{in } \Omega$$

and either natural boundary conditions

$$\frac{\partial\psi}{\partial\mathbf{n}} = \frac{\partial\rho}{\partial\mathbf{n}} = \frac{\partial c}{\partial\mathbf{n}} = \frac{\partial\mu}{\partial\mathbf{n}} = \frac{\partial v}{\partial\mathbf{n}} = \frac{\partial\omega}{\partial\mathbf{n}} = 0,\ \mathbf{u} = \mathbf{u}_\infty \ \text{ on } \partial\Omega,$$

where $\mathbf{n}$ denotes the outward normal vector or periodic boundary conditions.

III. NUMERICAL METHODS

An adaptive finite element method is used to solve the high-order nonlinear system of equations; the method is implemented using the adaptive finite element toolbox AMDiS.[38] We solve the coupled system as follows. First, the Cahn-Hilliard equations (31) and (32) are solved to determine the position of the interface, then the SPFC equations

(33)–(36) are solved to determine the surface colloid density and finally the Navier-Stokes equations (38) and (39) are solved to determine the fluid velocity using the new position of the interface and the surface density of the colloids in the surface tension and elastic forces. If colloids are present in the bulk, then the Eq. (37) is solved after the Navier-Stokes equation. To ensure the well-posedness of Eqs. (33)–(35), B is replaced by $B+\xi$ (see Ref. 29, for example). Analogously, in Eq. (37), ψ is replaced by $\psi+\xi$. Here, we use $\xi=10^{-6}$.

A semi-implicit Euler method is used for the time discretization keeping as many terms implicit as possible. Nonlinear terms are linearized by a Taylor expansion dropping terms of order two and higher so that the equations are linear at the implicit time step. The linearized system is solved using the direct unsymmetric multifrontal method [UMFPACK (Ref. 39)].

We use linear basis functions for all variables. Accordingly, the Cahn-Hilliard and SPFC equations are solved as coupled systems of second order equations (e.g., see Refs. 40 and 41). The Navier-Stokes equations are solved using a first order projection method developed in Ref. 42. The scheme is given by

$$\frac{\mathbf{u}^*-\mathbf{u}^{m-1}}{\tau}-\eta\Delta\mathbf{u}^*+\mathbf{u}^{m-1}\cdot\nabla\mathbf{u}^*=\mathbf{F}^m \tag{40}$$

$$\tau\Delta p^*=\nabla\cdot\mathbf{u}^* \tag{41}$$

$$\mathbf{u}^m:=\mathbf{u}^*-\tau\nabla p^* \tag{42}$$

where τ denotes the timestep and the superscripts denote the time iteration.

Adaptive meshes are indispensible for providing a high spatial resolution along the fluid-fluid interfaces described implicitly by ψ. For local mesh adaptation, we use a L^2-like error indicator based on a jump residual (e.g., see Refs. 38 and 43) for ψ to maintain approximately 5 grid points across the transition layers. Although we did not find it necessary to do here, additional mesh refinement can be used to increase local resolution of the flow field (e.g., velocity gradients, etc.).

IV. RESULTS

A. Retracting ellipse

As a first test for the NSCHSPFC model, we consider the case of an initially elliptical fluid droplet surrounded by another fluid. The computational domain is $\Omega=[-2,2]\times[-2,2]$ We start with an initial condition as in Eq. (2) using

$$d=1.0-\sqrt{\left(\frac{x}{0.35}\right)^2+\left(\frac{y}{1.8}\right)^2}.$$

Since this d is only an approximation to a signed distance function of an ellipse, we refine the initial condition by solving the Cahn-Hilliard equations (31) and (32) for a short time with velocity $\mathbf{u}=0$ to obtain better approximation of Eq. (2) where the actual signed distance function is used. The resulting ψ is the initial condition ψ_0 for the following simulations. It describes an elliptical drop with a vertical diameter of about 3 and a horizontal thickness of around 0.75.

To get an initial condition for ρ we solve the SPFC equations (33)–(36) on the fixed interface defined by ψ_0 (e.g., $\mathbf{u}$ is set to zero). We use as an initial condition for ρ a constant value of -0.3 plus a uniformly distributed random perturbation between $[-0.05,0.05]$ at each node. Hereafter, we write such a condition as $\rho_0=-0.3\pm0.05$ Since this surface density is in the crystal phase of the PFC, the colloidal particles become ordered and arrange in a crystal-like state. We stop solving the SPFC equations when a stationary state of colloid density is reached. The solution ρ shown in Fig. 1 is taken as the initial condition ρ_0 for the full NSCHSPFC system. Note that a single colloid corresponds to the combination of one darker region ($\rho<0$) and one lighter region ($\rho>0$). The remaining parameters are chosen as follows: $\tau=0.017$, $r=-0.4$, $\tilde{\rho}=0$, $Pe_\rho=3.76$, $Pe_\psi=0.47$, $Re=0.38$, $El=0.002$, $\epsilon=0.03$, $\delta=0.067$, and $Bi=0$, and the fluid is initially quiescent (e.g., $\mathbf{u}=0$ at time $t=0$). The natural boundary conditions with $\mathbf{u}_\infty=\mathbf{0}$ are used.

Fig. 2 shows the NSCHSPFC simulation (bottom) and a comparison to the Navier-Stokes-Cahn-Hilliard (NSCH) model (top) which has no elastic force ($El^{-1}=0$). One can see that in the latter case surface tension makes the ellipse retract to become circular. However, in the presence of colloids, the retraction is stopped by the elastic force as the colloids jam at the interface and the interface crystallizes. Note that at late times, the interface may start to wobble a little. This is likely due to the combination of the surface elasticity induced by the colloids and the inertial forces in the fluid.

The velocity $\mathbf{u}$ at the top of the ellipse at an early time ($t=1.67$) is shown in Fig. 3 . The elastic force induces local straining flows around the interface (two per colloid). The maximum magnitudes of the velocities induced by the surface tension and elastic force are about ten times larger than that induced by the surface tension only. Consequently, we need to use smaller time steps and a finer grid in a neighborhood of the interface to resolve the system with elastic forces

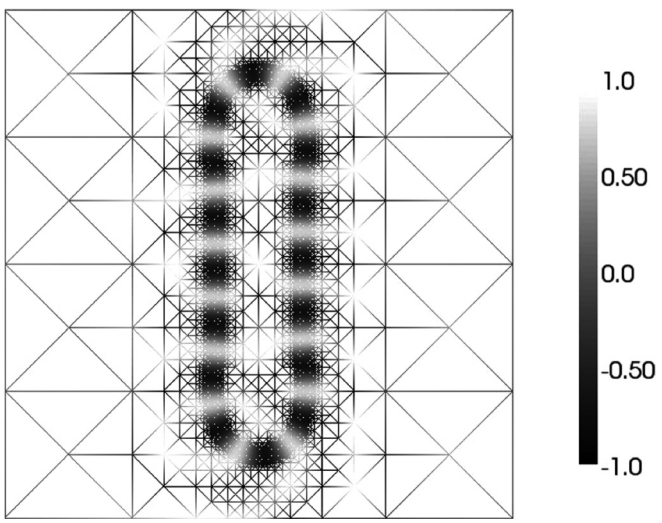

FIG. 1. Initial condition ρ_0 for the NSCHSPFC system obtained by solving the SPFC equation on an elliptical diffuse interface, as described in the text.

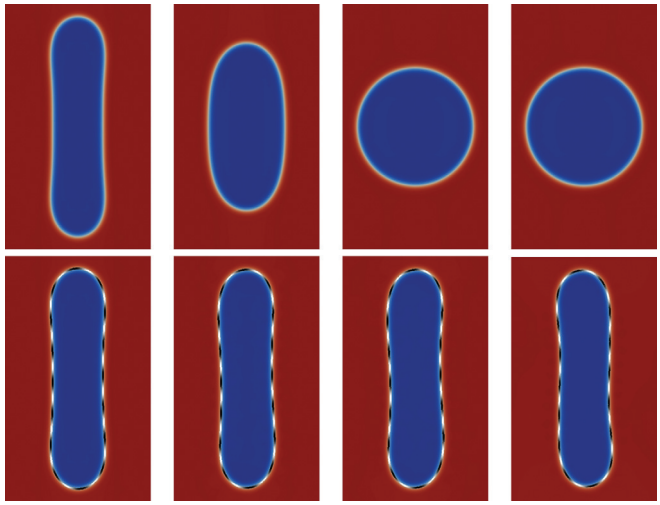

FIG. 2. (Color online) Retraction of an elliptical drop without (top) and with (bottom) colloidal forces at times $t = 0, 33, 167,$ and 1671 from left to right. The drop and matrix fluids have different shades, lighter (red online) for $\psi = 1$ and darker (blue online) for $\psi = 0$ The colloids (ρ) on the interface are colored black ($\rho < 0$) and white ($\rho > 0$).

than are required to solve the system without elastic forces. The magnitude of the straining flows can be decreased by increasing El. To compensate for an increased El, the number of colloids on the interface may be increased, which increases the interface stiffness by enabling colloid jamming and interface crystallization to occur more readily. This can be achieved by making the colloidal particles smaller resulting in a smaller parameter δ, as we now demonstrate.

To investigate the influence of the number of colloids on the system, we vary the parameter δ, which relates the characteristic colloid size to the characteristic drop radius. Now, we proceed as before. We first solve the SPFC equation on a fixed interface until a stationary state is reached. We use three values of $\delta = 0.133$, 0.067 and 0.033. This yields 8, 16, and 32 colloids on the interface as seen in Fig. 4. Using the same parameters and boundary conditions as before, with the exception of δ, the initial ellipses are evolved in time in an initially quiescent fluid. In Fig. 5, the interface length, calculated by from the length of the $\psi = 0.5$ contour, is plotted as a function of time. In all cases, the elastic force is strong enough to stop the retraction, with the decrease in length being inversely proportional to δ. Thus, increasing the number of colloids makes the interface stiffer by making it easier for the colloids to jam. Note that for $\delta = 0.133$, a minimum in interface length occurs around time $t \approx 50$ as the drop

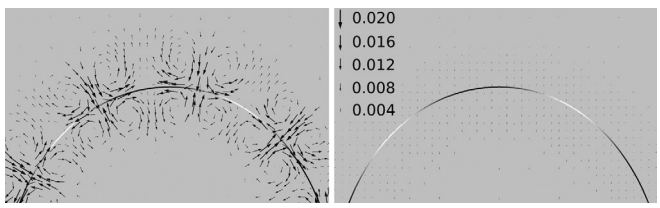

FIG. 3. Velocity field at the top of the ellipse at the early time $t = 1.67$. The black-white curve represents the interface. Left: The NSCHSPFC system induces localized straining flows along the interface. Right: The velocity induced by surface tension only (elastic force turned off, $El^{-1} = 0$), at the same time, for comparison.

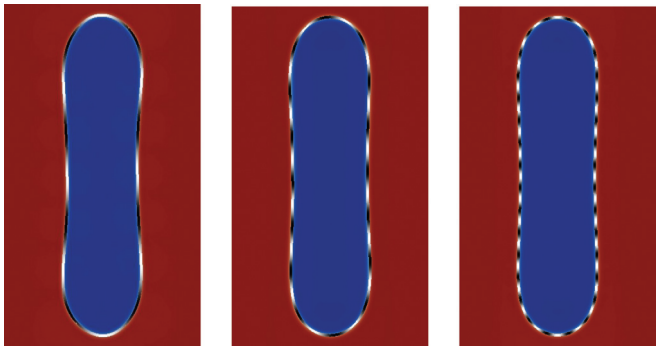

FIG. 4. (Color online) Drop morphologies with 8, 16, and 32 colloids at the interface used as initial condition for the NSCHSPFC model.

starts to retract to a circle; its length only decreases by only about 1% though. After this, the particles seem to slightly over compress and the drop rebounds a little to an equilibrium configuration. This occurs to a much lesser extent for the case with 16 colloids. In the case, with 32 colloids, the interface length evolves monotonically with very slight decrease in length. To reach the smaller values of δ needed to model specific experiments (e.g., Refs. 9, 14, and 15), larger scale simulations are necessary. This is currently research in progress.

Next, we incorporate attachment into the system. Therefore, we solve an additional concentration equation as described in Sec. II B. As initial condition, we impose a colloid concentration in the lower region of the domain:

$$c_0(x, y) = \begin{cases} 1, & \text{if } y < -1.67 \\ 0, & \text{else.} \end{cases}$$

The parameters are the same as before, with $\delta = 0.067$, and the parameters associated with attachment are $Bi = 0.6$, $k^{-1} = 0$, $Pe_c = 37.6$, $h = 0.67$ and $\rho_\infty = 0.0$. The initial surface colloid density $\rho_0 = -0.8$, which is in the liquid phase of the PFC (e.g., the colloid phase is disordered). Thus, attachment is needed to order the colloids and crystallize the interface. Accordingly, the surface colloid structure evolves dynamically together with the interface evolution and attachment from the bulk matrix fluid. The results, shown in Figure 6, show that colloids attach to and crystallize the interface

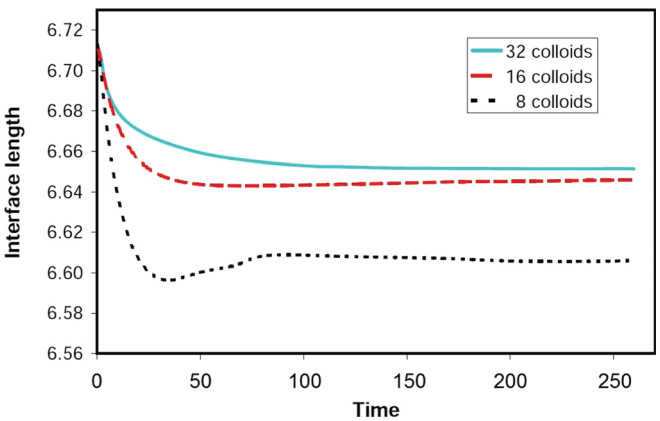

FIG. 5. (Color online) Interface length as a function of time for different numbers of colloids on the interface (see text for details).

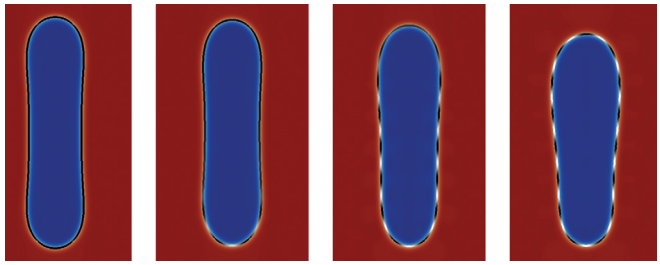

FIG. 6. (Color online) Retraction of an elliptical drop with simulated attachment of colloids. From left to right, the times shown are $t = 0$, 3.3, 10.0, and 33.4.

starting at the bottom of the ellipse (closest to the bulk source) and move upwards as time progresses. Correspondingly, the retraction stops first at the bottom of the ellipse, since the colloids jam there first, with the retraction becoming progressively more arrested as the colloid structure moves up the ellipse. This leads to the development of an asymmetrical shape because the drop retracts more at the top.

B. Drop in shear flow

We consider a drop in shear flow to show that the colloids on the interface induce both repulsive and attractive forces. This ability to impart rigidity, akin to surface elasticity, is an important difference between colloid stabilized and surfactant stabilized systems. Surfactants can lower the surface tension but they do not generally result in significant surface elasticity. This makes it easier for colloid stabilized systems to resist external forces such as arise in an externally applied shear flow.

To illustrate this, we simulated a drop with colloids and elastic force (NSCHSPFC), a drop without colloids (NSCH), and a drop without colloids but with insoluble surfactants on its surface. The latter is performed using the diffuse-interface formulation in Teigen *et al.*,[32] which we briefly describe. The surfactant concencentration c_s on the interface satisfies

$$\partial_t(Bc_s) + \nabla\cdot(B\mathbf{u}c_s) = \frac{1}{Pe_{c_s}}\nabla\cdot(B\nabla c_s), \tag{43}$$

where Pe_{c_s} is the surfactant Peclet number. The nondimensional surface tension (scaled by the clean surface tension) is dependent on c_s using the linear approximation

$$\sigma_s = (1-\beta c_s) \tag{44}$$

with a constant factor β. The capillary and Marangoni forces are accounted for by using the following force in the Navier-Stokes equation

$$\mathbf{F} = (1-\beta c_s)\frac{\delta E_s}{\delta\psi}\nabla\psi - \frac{\sqrt{2}}{6}\beta|\nabla\psi|\left(\mathbf{I} - \frac{\nabla\psi\otimes\nabla\psi}{|\nabla\psi|^2}\right)\nabla c_s, \tag{45}$$

where the $\sqrt{2}/6$ arises in order to match the scaling of the different delta function representations used in the two terms. An asymptotic analysis as $\epsilon\to 0$ reveals that the first term tends to $-\frac{\sqrt{2}}{6}(1-\beta c_s)\kappa\delta_\Sigma\mathbf{n}$ with κ the total curvature of Γ (e.g., see Ref. 44). In the second term $|\nabla\psi| \sim \delta_\Gamma$ and thus the scaling is needed in order to balance the terms to approximate the sharp interface limit $\frac{6}{\sqrt{2}}\mathbf{F} \sim -(1-\beta c_s)\kappa\delta_\Gamma\mathbf{n} - \beta\nabla_s c_s\delta_\Gamma$.

In our simulations, we use $\beta = 0.5$, $Pe_{c_s} = 39$ and the initial condition $c_s = 1.0$. Here, the domain size is $\Omega = [-6,6]\times[-2,2]$ and a drop of radius 1 is placed in the center. To obtain an initial configuration with colloids on the interface, we solve the SPFC equations first on this fixed interface to steady state starting from an initial colloid density $\rho_0 = -0.3\pm 0.05$. This creates a stationary state with 15 colloids at the circular interface. Note that there are fewer colloids here than in the elliptical case considered previously since the interface length is smaller. This solution ρ is taken as the initial condition for the complete NSCHSPFC system. We take $\tau = 0.0084$, $El = 4\times 10^{-4}$, $\delta = 0.067$, $Bi = 0$ and the remaining parameters as in Sec. IV A. We use periodic boundary conditions on the left and right boundaries of the domain. At the top and bottom boundaries, the natural boundary conditions are used with $\mathbf{u}_\infty = (0.24, 0)$ and $\mathbf{u}_\infty = (-0.24, 0)$ respectively. The initial fluid velocity is $\mathbf{u}_0 = (0.12y, 0)$.

The result is shown in Fig. 7. The drop with colloids (black and white) deforms only slightly and reaches a steady morphology around time $t = 10$ and thereafter resists deformation by the shear flow. In contrast, the drop with surfactants (grey) and the clean drop without colloids and surfactants ($\beta = 0$, $El^{-1} = 0$ black) increasingly elongate in time. As expected the drop with surfactants deforms the most.

C. Stabilizing bicontinuous structures

We next investigate the potential of colloidal particles to stabilize the bicontinuous structures generated by spinodal

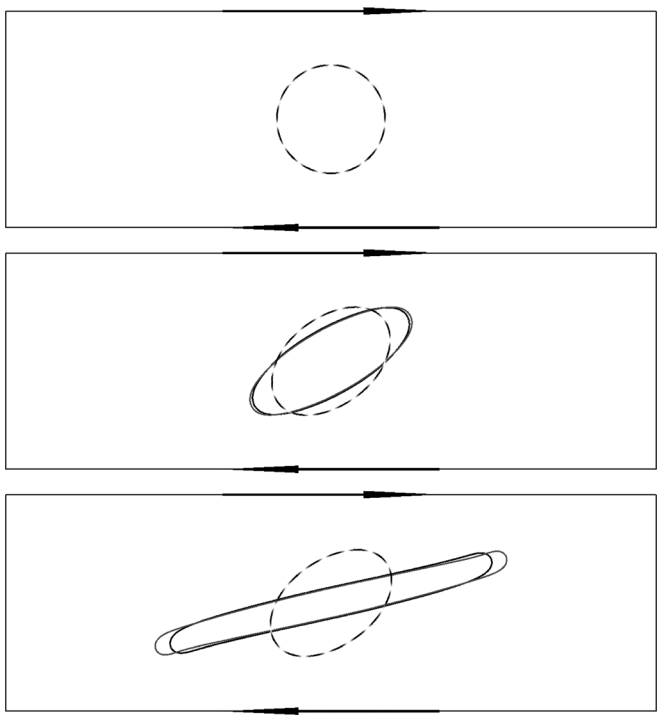

FIG. 7. A drop under shear flow. With colloids (black-white), without colloids (black), and with insoluble surfactants on the interface (grey) at times $t = 0$, 10.0, and 33.4.

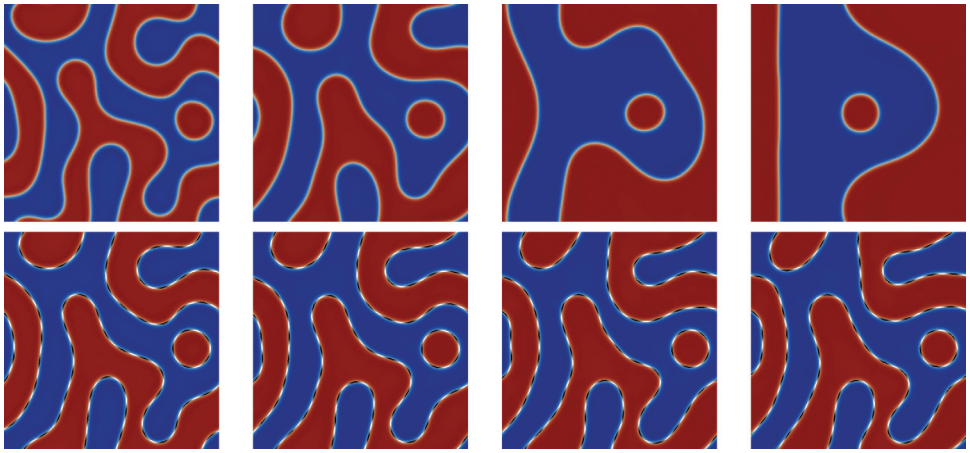

FIG. 8. (Color online) The evolution of a complex fluid structure generated by spinodal decomposition without (top) and with (bottom) colloidal forces at times $t = 0$, 16.7, 83.6, and 167 from left to right. The presence of colloids arrests the coarsening.

decomposition in the computational domain $[-2,2]\times[-2,2]$ We first attempted to model this by solving the full NSCHSPFC system using an initial condition in which the fluid is quiescent, no interface is present (e.g., $\psi = 0.5 \pm 0.1$) and colloids are only present in the bulk. Thus, the interface crystallization should arise from attachment of colloids at the interface as it nucleates and coarsens. However, we found that the fluid phases never reached a steady, stable state due to the competing effects between the sizes of the fluid structures that form at early times and the colloid sizes. In particular, the fluid structures should be larger than the size of the colloids (e.g., $\delta < 1$).

As an alternative initial condition, we first generate sufficiently large fluid structures via spinodal decomposition by solving the CH equation in the absence of flow ($\mathbf{u} = 0$) using the initial condition for ψ mentioned above, with a large interface thickness $\epsilon = 0.16$ for a few time steps. Then, to generate the initial condition for the full NSCHSPFC system, the CH and SPFC equations are solved together for several more time steps, again in the absence of flow, with $\epsilon = 0.03$ to refine the interface thickness and to create the colloid structure on the complex interface. As initial data for the CH-SPFC solve, the previously generated ψ is used together with the colloid density $\rho_0 = -0.3 \pm 0.05$. The resulting ψ, ρ are used as the initial condition ψ_0, ρ_0 for the full NSCHSPFC system. The parameters are the same as in Sec. IV A with $\delta = 0.067$; periodic boundary conditions are used in each coordinate direction.

Figure 8 shows a comparison between the NSCHSPFC model (bottom) and a NSCH model without the elastic force ($El^{-1} = 0$, top). In the latter case, the structure coarsens significantly. When colloids are present, the elastic force induced by the particles is able to prevent the coarsening as the colloids jam and the interface crystallizes. Indeed, it can be seen in Fig. 10 the interface length (long-dashed) decreases only slightly throughout the simulation. In contrast, without colloids, the interface length decreases substantially over the simulation (solid). Hence, the colloids stabilize the system against coarsening.

D. Stabilizing bicontinuous structures using coarsening-induced jamming

Next, we simulate the jamming of colloids at the interface as proposed in Sec. II C. In particular, using the same initial interfacial configuration in Sec. IV C, we start with an unordered colloid configuration. We test whether ordering and crystallization of the interface may occur as the complex fluid structure coarsens. As discussed in Sec. II C, we introduce a shifting constant $\tilde{\rho}$ to shift the crystal region of the PFC phase diagram. Here, we take $\tilde{\rho} = 1$ which makes the crystalline phase of the PFC occur near densities $\rho \approx 1$. The initial SPFC density is $\rho_0 = 0.35$, ψ_0 and the remaining parameters as the same as in Sec. IV C.

The results are shown in Fig. 9. At early times, the fluid structure coarsens and the NSCHSPFC evolution is very similar to that for the NSCH system without colloids (Fig. 8 (top)). At these early times, the interface has not yet crystallized. Therefore, the elastic force is small and the evolution is dominated by the surface tension force. As the interface coarsens, the colloid density increases and eventually reaches the limit where the colloids jam and the interface crystallizes. This occurs around time $t \approx 60$ and crystallization begins in the upper right portion of the interface first. The crystal region then spreads rapidly around the interface. Interestingly, although the coarsening slows significantly after the initial crystallization, the increased elastic forces do not immediately stop the coarsening because there are some adjustments in the colloid distribution that result in changing the local colloid density (particularly at the upward pointing

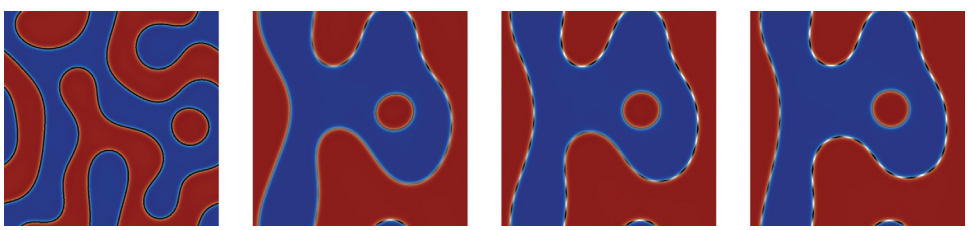

FIG. 9. (Color online) Coarsening of a complex fluid structure with simulated jamming of colloids. The times shown are $t = 0$, 58.5, 83.6, and 167 from left to right.

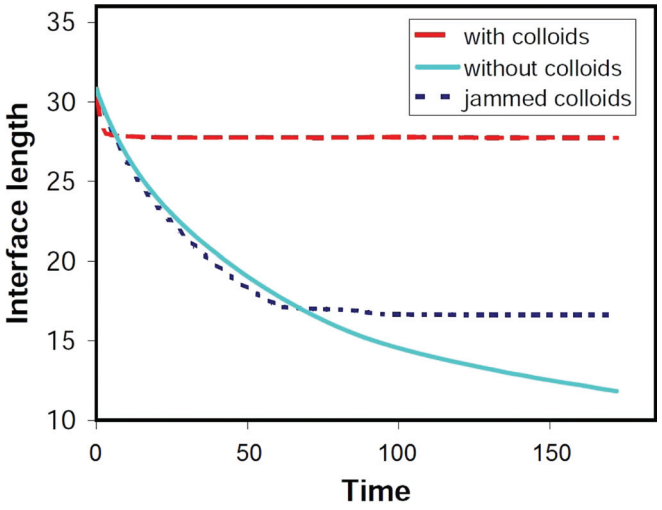

FIG. 10. (Color online) The evolution of the interface length for the simulations shown in Figures 8 and 9. Without elastic force (solid line), with elastic force from the beginning (long-dashed), and with elastic force where the colloids jam and the interface crystallizes during coarsening (short-dashed).

finger in the center of the domain). This results in a small amount of additional localized coarsening. As the colloid density equilibrates and the colloids jam fully, the coarsening of the fluid structure ceases. Note that crystallization does not occur on the isolated drop because the drop is nearly circular and thus does not coarsen enough to increase the colloid density to the crystallization limit.

To quantify the coarsening process, the total interface length (calculated as described earlier) is plotted in Fig. 10 as a function of time for the three simulations modeling the bicontinuous structures (Figs. 8 and 9). At early times, before the interface crystallizes, the interface length for the simulation shown in Fig. 9 (short dashed) evolves very similarly as the case without colloids ($El^{-1} = 0$, solid). Thus, the elastic force seems to have almost no effect on the system if the surface colloid density is in the liquid phase. The point at which the colloids start to jam and the interface begins to crystallize is clearly indicated by the abrupt stop in the decrease of the interface length around $t \approx 60$. The additional localized coarsening that occurs in response to colloid redistribution is seen by the slight decrease in interface length around $t \approx 80$. After the colloids jam fully, the interface length stays almost perfectly constant.

V. CONCLUSIONS

We have developed a model to simulate the presence of colloids at interfaces in a two-phase system. Our approach combines a Navier-Stokes-Cahn-Hilliard model for a macroscopic two-phase system with a surface phase-field-crystal model for the microscopic colloidal system along the interface. In the resulting NSCHSPFC model, the presence of colloids introduces elastic forces at the interface between the two immiscible fluid phases. On the interface, colloids induce both repulsive and attractive forces, which can make the interface rigid. This ability to impart rigidity, akin to surface elasticity, is an important difference between colloid stabilized and surfactant stabilized systems. An adaptive finite element method is used to solve the model numerically. Using a variety of flow configurations in two dimensions, we demonstrated that as colloids jam on the interface and the interface crystallizes, the elastic force may be strong enough to make the interface sufficiently rigid to resist external forces, such as an applied shear flow, as well as surface tension induced coarsening. Although one may be tempted to associate this behavior with a divergence of the interfacial viscosity (e.g., a surface version of the Krieger-Dougherty equations[45]) rather than colloid jamming, the surface viscosity interpretation cannot support equilibrium solutions that may exist in a state of stress analogous to capillary stresses for colloid-free interfaces. This suggests that jamming interactions among the colloids are responsible for halting the interface motion.

We presented examples where the interface is crystallized initially and where crystallization and jamming are induced by attachment of colloids from the bulk. We also presented an example of coarsening-induced colloid jamming resulting in a bijel. In this example, the coarsening of a two-dimensional bicontinuous structure under surface tension forces raises the colloid density sufficiently to induce jamming, which abruptly halts the coarsening process.

There are many interesting directions to pursue in the future, the first of which should be an extension of this approach to three dimensions and to incorporate large scale simulations capable of resolving very small values of δ needed to simulate experimental conditions. While the NSCHSPFC model and the numerical method for the NSCH part of the model extend straightforwardly to three dimensions, the numerical method for the SPFC equation needs to be improved. For example, using the direct method UMFPACK to solve the linearized system is too expensive in three dimensions. To make the method more efficient, we are currently developing iterative methods and parallel implementations for use in two and three dimensions. Other directions, we are currently pursuing include developing methods to upscale the microscopic SPFC model and elastic force to obtain a fully macroscopic system, investigating the rheological properties of simulated bijels and comparing the results with physical systems (e.g., Refs. 46 and 47), and developing a model of a crossflow microreactor in which two fluids flow in opposite direction allowing close contact between mutually insoluble reagents across a colloid-stabilized interface in a bijel.[10]

ACKNOWLEDGMENTS

S.A. and A.V. acknowledge support from the German Science Foundation through Grant Nos. Vo899/6-1 and SFB 609. J.L. gratefully acknowledges partial support from the National Science Foundation Division of Mathematical Sciences and the Division of Materials Research.

APPENDIX: NONDIMENSIONALIZATION

Consider the dimensional energy for the colloid-fluid system

$$E = E_{kin} + E_s + E_{spfc}, \tag{A1}$$

with the dimensional kinetic and surface energies given by

$$E_{kin} = \frac{\bar{\rho}}{2}\int |\mathbf{u}|^2 dx, E_s = \sigma \int \frac{1}{\epsilon}\left(B(\psi) + \epsilon^2 |\nabla\psi|^2\right) dx, \quad \text{(A2)}$$

where $\bar{\rho}$ is the constant density of the fluid, and σ is a surface tension coefficient. The dimensional SPFC energy is given by

$$E_{spfc} = \lambda \int \frac{1}{\epsilon} B(\psi) f(\phi) dx, \quad \text{(A3)}$$

where λ is an elastic energy coefficient and the SPFC energy density f is given by

$$f(\phi) = \frac{\phi^2}{2}\left(a + \tilde{\beta} q_0^4\right) + \frac{g}{4}\phi^4 - \tilde{\beta} q_0^2 |\nabla\phi|^2 + \frac{\tilde{\beta}}{2}\left(\frac{1}{B(\psi)}\nabla\cdot(B(\psi)\nabla\phi)\right)^2. \quad \text{(A4)}$$

The function ϕ is a dimensionless measure of the colloidal density field (e.g., $\phi = \left(\rho_{crys} - \bar{\rho}_{crys}\right)\big)/\bar{\rho}_{crys}$ where ρ_{crys} is the colloid density and $\bar{\rho}_{crys}$ is a reference density, for example, the density of the system in the liquid state). The quantities a, $\tilde{\beta}$, q_0, and g are system specific parameters. The first three can be determined from matching the liquid structure factor for the colloidal system with q_0^{-1} setting the crystal lattice spacing, and a and $\tilde{\beta}$ being determined by a polynomial approximation to the liquid structure factor. The remaining parameter g can be determined by fixing the amplitude of density waves in the crystal state. See Refs. 23, 25, 28, and 48, for example, where the connections between the PFC model and the classical DDFT are also discussed.

Introducing characteristic scales for space L (e.g., characteristic drop radius) and velocity $U = \sqrt{\sigma/(\bar{\rho}L)}$ (e.g., the characteristic surface tension velocity), we define the nondimensional quantities denoted by tildes

$$\tilde{\mathbf{x}} = \mathbf{x}/L, \tilde{t} = tU/L, \tilde{\mathbf{u}} = \mathbf{u}/U, \tilde{E} = E/(\bar{\rho}U^2L^3) \quad \text{(A5)}$$

and

$$r = a/(\tilde{\beta}q_0^4), \tilde{\epsilon} = \epsilon/L, \delta = 1/(Lq_0), \quad \text{(A6)}$$

we get the nondimensional energies

$$\tilde{E}_{kin} = \frac{1}{2}\int |\tilde{\mathbf{u}}|^2 d\tilde{x}, \tilde{E}_s = \frac{1}{\tilde{\epsilon}}\int B(\psi) + \tilde{\epsilon}^2 |\tilde{\nabla}\psi| d\tilde{x}. \quad \text{(A7)}$$

Taking $\rho = \sqrt{\frac{g}{\tilde{\beta}q_0^4}}\phi$ (e.g., see also Ref. 49), the nondimensional PFC energy becomes

$$\tilde{E}_{spfc} = \frac{El^{-1}}{\tilde{\epsilon}}\int B(\psi) f(\rho) d\tilde{x}, \quad \text{(A8)}$$

where $El = \frac{\bar{\rho}U^2L}{\lambda}\cdot\frac{g}{\tilde{\beta}q_0^8} = \frac{\sigma}{\lambda}\cdot\frac{g}{\tilde{\beta}q_0^8}$ is an elasticity number that measures the strength of the SPFC energy relative to the surface energy, and

$$f(\rho) = \frac{\rho^4}{4} + \frac{\rho^2}{2}(1+r) - \delta^2|\widetilde{\nabla}\rho|^2 + \frac{\delta^4}{2}\left(\frac{1}{B(\psi)}\widetilde{\nabla}\cdot\left(B(\psi)\widetilde{\nabla}\rho\right)\right)^2. \quad \text{(A9)}$$

[1] P. S. Clegg, E. M. Herzig, A. B. Schofield, S. U. Egelhaaf, T. S. Horozov, B. P. Binks, M. E. Cates, and W. C. K. Poon, "Emulsification of partially miscible fluids using colloidal particles: Nonspherical and extended domain structures," Langmuir **23**, 5984 (2008).
[2] P. S. Clegg, "Fluid-bicontinuous gels stabilized by interfacial colloids: Low and high molecular weights," J. Phys. Condens. Matter **20**, 113101 (2008).
[3] A. B. Subramaniam, M. Abkarian, L. Mahadevan, and H. A. Stone, "Nonspherical bubbles," Nature **438**, 930 (2005).
[4] S. Pickering, "Emulsions," J. Chem. Soc. **91**, 2001 (1907).
[5] C. Zeng, H. Bissig, and A. D. Dinsmore, "Particles on droplets: From fundamental physics to novel materials," Solid State Commun. **139**, 547 (2006).
[6] F. Leal-Calderon and V. Scmitt, "Solid-stabilized emulsions," Curr. Opin. Colloid Interface Sci. **13**, 217 (2008).
[7] E. Dickinson, "Solid-stabilized emulsions," Curr. Opin. Colloid Interface Sci. **15**, 40 (2010).
[8] M. E. Cates and P. S. Clegg, "Bijels: A new class of soft materials," Soft Matter **4**, 2132 (2008).
[9] H. J. Chung, K. Ohno, T. Fukuda, and R. J. Composto, "Self-regulated structures in nanocomposites by directed nanoparticle assembly," Nano Lett. **5**, 1878 (2005).
[10] K. Stratford, R. Adhikari, I. Pagonabarraga, J. C. Desplat, and M. E. Cates, "Colloidal jamming at interfaces: A route to fluid-bicontinuous gels," Science **309**, 2198 (2005).
[11] M. Ulbricht, "Advanced functional polymer membranes," Polymer **47**, 2217 (2006).
[12] W. L. Ma, C. Y. Yang, X. Gong, K. Lee, and A. J. Heeger, "Thermally stable, efficient polymer solar cells with nanoscale control of the interpenetrating network morphology," Adv. Funct. Mater. **15**, 1617 (2005).
[13] E. Sanz, K. A. White, P. S. Clegg, and M. E. Cates, "Colloidal gels assembled via a temporary interfacial scaffold," Phys. Rev. Lett. **103**, 255502 (2009).
[14] E. M. Herzig, K. A. White, A. B. Schofield, W. C. Poon, and P. S. Clegg, "Bicontinuous emulsions stabilized solely by colloidal particles," Nature Mater. **6**(12), 966, (2007).
[15] H. Firoozmand, B. S. Murray, and E. Dickinson, "Interfacial structuring in a phase-separating mixed biopolymer solution containing colloidal particles," Langmuir **25**, 1300 (2009).
[16] E. Kim, K. Stratford, R. Adhikari, and M. E. Cates, "Arrest of fluid demixing by nanoparticles: A computer simulation study," Langmuir **24**, 6549 (2008).
[17] M. J. A. Hore and M. Laradji, "Microphase separation induced by interfacial segregation of isotropic spherical nanoparticles," J. Chem. Phys. **126**, 244903 (2007).
[18] U. M. B. Marconi and P. Tarazona, "Dynamical density functional theory of liquids," J. Chem. Phys. **110**, 8032 (1999).
[19] A. J. Archer and M. Rauscher, "Dynamic density functional theory for interacting brownian particles: Stochastic or deterministic?," J. Phys. A **37**, 9325 (2004).
[20] I. Napari, A. Laaksonen, and R. Strey, "Density-functional studies of amphiphilic binary mixtures," J. Chem. Phys. **113**, 4476 (2000).
[21] P. S. Christopher and D. W. Oxtoby, "Density functional model of surfactant mesostructures," J. Chem. Phys. **117**, 9502 (2002).
[22] A. J. Archer, "Dynamical density functional theory for molecular and colloidal fluids: A microscopic approach to fluid mechanics," J. Chem. Phys. **130**, 014509 (2009).
[23] S. van Teeffelen, R. Backofen, A. Voigt, and H. Löwen, "Derivation of the phase-field-crystal model for colloidal solidification," Phys. Rev. E **79**(5), 051404 (2009).
[24] K. R. Elder, M. Katakowski, M. Haataja, and M. Grant, "Modeling elasticity in crystal growth," Phys. Rev. Lett. **88**, 245701 (2002).
[25] K. R. Elder, N. Provatas, J. Berry, P. Stefanovic, and M. Grant, "Phase-field crystal modeling and classical density functional theory of freezing," Phys. Rev. B **75**(6), 064107 (2007).
[26] N. Provatas, J. A. Dantzig, B. Athreya, P. Chan, P. Stefanovic, N. Goldenfeld, and K. Elder, "Using the phase-field crystal method in the multiscale modeling of microstructure evolution," JOM **59**, 83 (2007).
[27] N. Provatas and K. Elder, *Phase-field Methods in Materials Science and Engineering* (Wiley-VCH, Weinheim, Germany, 2010).
[28] R. Backofen, T. Witkowski, and A. Voigt, "Particles on curved surfaces—A dynamic approach by a phase field crystal model," Phys. Rev. E **81**, 025701R (2010).
[29] A. Rätz, and A. Voigt, "PDE's on surfaces—A diffuse interface approach," Commun. Math. Sci. **4**, 575 (2006).

[30]X. Li, J. S. Lowengrub, A. Rätz, and A. Voigt, "Solving PDEs in complex geometries: A diffuse domain approach," Commun. Math. Sci. **7**, 81 (2009).
[31]K. E. Teigen, X. Li, J. Lowengrub, F. Wang, and A. Voigt, "A diffuse-interface approach for modeling transport, diffusion and adsorption/desorption of material quantities on a deformable interface," Commun. Math. Sci. **7**, 1009 (2009).
[32]K. E. Teigen, P. Song, J. Lowengrub, and A. Voigt, "A diffuse interface method for two-phase flows with soluble surfactants," J. Comput. Phys. **230**, 375 (2010).
[33]D. M. Anderson, G. B. McFadden, and A. A. Wheeler, "Diffuse interface methods in fluid mechanics," Annu. Rev. Fluid Mech. **30**, 139 (1998).
[34]I. Singer-Loginova and H. Singer, "The phase field technique for modeling multiphase materials," Rep. Prog. Phys. **71**, 106501 (2008).
[35]H. Emmerich, "Advances of and by phase-field modeling in condensed-matter physics," Adv. Phys. **57**, 1 (2008).
[36]J. W. Cahn and J. E. Hilliard, "Free energy of a nonuniform system. I. Interfacial free energy," J. Chem. Phys. **28**, 258 (1958).
[37]J. Swift and P. C. Hohenberg, "Hydrodynamic fluctuations at convective instability," Phys. Rev. A **15**, 319 (1977).
[38]S. Vey and A. Voigt, "Amdis: Adaptive multidimensional simulations," Comput. Visualization Sci. **10**(1), 57 (2007).
[39]T. Davis, "Users' guide for the unsymmetric-pattern multifrontal package (umfpack)," Technical Report No. TR-95-004 (Computer and Information Sciences Department, University of Florida, Gainesville, FL, 1995).
[40]S. Aland, J. S. Lowengrub, and A. Voigt, "Two-phase flow in complex geometries: A diffuse domain approach," Comput. Model. Eng. Sci. **57**, 77 (2010).
[41]R. Backofen, A. Ratz, and A. Voigt, "Nucleation and growth by a phase field crystal (PFC) model," Philos. Mag. Lett. **87**, 813 (2007).
[42]A. J. Chorin, "Numerical solution of the Navier-Stokes equations," Math. Comput. **22**, 745 (1968).
[43]R. Verfürth, *A Review of a Posteriori Error Estimation and Adaptive Mesh-refinement Techniques*, Wiley-Teubner Series Advances in Numerical Mathematics, Vol. VI, edited by B. G. Teubner (Wiley, Chichester, 1996), p.127.
[44]J. Lowengrub and L. Truskinovsky, "Quasi-incompressible Cahn-Hilliard fluids and topological changes," Proc. R. Soc. London, Ser. A **454**, 2617 (1998).
[45]I. M. Krieger and T. J. Dougherty, "Efficient numerical solution of Cahn-Hilliard-Navier-Stokes fluids in 2d," Trans. Soc. Rheol. **3**, 137 (1959).
[46]P. Cicuta, E. J. Stancik, and G. G. Fuller, "Shearing or compressing a soft glass in 2d: Time-concentration superposition," Phys. Rev. Lett. **90**, 236101 (2003).
[47]S. Reynaert, P. Moldenaers, and J. Vermant, "Interfacial rheology of stable and weakly aggregated two-dimensional suspensions," Phys. Chem. Chem. Phys. **9**, 6463 (2007).
[48]K. A. Wu and A. Karma, "Phase-field crystal modeling of equilibrium bcc-liquid interfaces," Phys. Rev. B **76**, 184107 (2007).
[49]K.-A. Wu and P. W. Voorhees, "Stress-induced morphological instabilities at the nanoscale examined using the phase field crystal approach," Phys. Rev. B **80**, 125408 (2009).